

Energy-Constrained UAV Data Collection Systems: NOMA and OMA

Xidong Mu, *Graduate Student Member, IEEE*, Yuanwei Liu, *Senior Member, IEEE*, Li Guo, *Member, IEEE*, Jiaru Lin, *Member, IEEE*, and Zhiguo Ding, *Fellow, IEEE*

Abstract—This paper investigates unmanned aerial vehicle (UAV) data collection systems with different multiple access schemes, where a rotary-wing UAV is dispatched to collect data from multiple ground nodes (GNs). Our goal is to maximize the minimum UAV data collection throughput from GNs for both orthogonal multiple access (OMA) and non-orthogonal multiple access (NOMA) transmission, subject to the energy budgets at both the UAV and GNs, namely *double energy limitations*. 1) For OMA, we propose an efficient algorithm by invoking alternating optimization (AO) method, where each subproblem is alternately solved by applying successive convex approximation (SCA) technique. 2) For NOMA, we first handle subproblems with fixed decoding order using SCA technique. Then, we develop a penalty-based algorithm to solve the decoding order design subproblem. Numerical results show that: i) The proposed algorithms are capable of improving the max-min throughput performance compared with other benchmark schemes; and ii) NOMA yields a higher performance gain than OMA when GNs have sufficient energy.

I. INTRODUCTION

Recently, unmanned aerial vehicles (UAVs) or drones have received extensive attention in military and civil applications with the advantages of low cost, high maneuverability, and high mobility [1]. Equipped with communication devices, UAVs can act as aerial base stations (BSs) or users for accomplishing variant tasks, such as communication enhancement and offloading, cargo delivery, and security surveillance [2–4]. Among others, UAV data collection has been envisioned as a promising application, where UAVs equipped with sensing devices are deployed to collect data from ground nodes (GNs) [5]. Compared with terrestrial data collection systems, on the one hand, GNs are able to upload data to UAVs directly through the line-of-sight (LoS) dominated UAV-ground channels [6], thus reducing energy consumptions of GNs and improving the transmission efficiency. On the other hand, thanks to the low cost and high flexibility features of UAVs, UAV data collection systems are more suitable to be

used in inaccessible regions, such as forest or marine monitoring, where deploying conventional terrestrial infrastructure to collect data is costly and inefficient.

Multiple access (MA) technique is one of the most fundamental enablers for facilitating UAV data collection systems since the number of GNs is usually large. The existing MA techniques can be loosely classified into two categories, namely, orthogonal multiple access (OMA) and non-orthogonal multiple access (NOMA). Different from OMA where one resource block (in time, frequency, or code) is occupied with at most one user, the key idea of NOMA¹ is to allow different users to share the same time/frequency resources and to be multiplexed in different power levels by invoking superposition coding and successive interference cancellation (SIC) techniques [7, 8]. Owing to flexible resource allocations, NOMA is capable of improving spectrum efficiency, supporting massive connectivity, and guaranteeing user fairness [7]. Recall that the diversified communication demands and massive connectivity requirements of UAV data collection systems, it is natural to investigate the employment of NOMA in UAV data collection systems and explore the potential performance gain.

A. Related Works

1) *Studies on UAV Communication Systems*: UAV communication systems have drawn significant attention of researchers in the past few years. In existing literature, UAVs are deployed as aerial BSs, relays, and users to boost the performance of communication systems, such as coverage and capacity. In terms of UAVs' state in the sky, research contributions can be divided into two categories: static UAV and mobile UAV communication systems. For static UAV communication systems, researchers mainly focused on the optimal deployment/placement of UAVs due to the unique air-to-ground (A2G) channel characteristics. The authors of [9] studied the optimal UAV altitude to maximize the coverage based on the probability A2G channel model. The authors of [10] further investigated optimal three-dimensional (3D) deployment of multiple UAVs, where an efficient method was proposed to achieve the maximum coverage while considering the inter-cell interference caused by different UAVs. The authors of [11] proposed a spiral-based algorithm with the aim of using the minimum number of UAVs to ensure that all

Copyright (c) 2015 IEEE. Personal use of this material is permitted. However, permission to use this material for any other purposes must be obtained from the IEEE by sending a request to pubs-permissions@ieee.org.

X. Mu, L. Guo, and J. Lin are with the Key Laboratory of Universal Wireless Communications, Ministry of Education, Beijing University of Posts and Telecommunications, Beijing 100876, China, and are also with the School of Artificial Intelligence, Beijing University of Posts and Telecommunications, Beijing 100876, China. (email: {muxidong, guoli, jrlin}@bupt.edu.cn).

Y. Liu is with the School of Electronic Engineering and Computer Science, Queen Mary University of London, London, UK. (email: yuanwei.liu@qmul.ac.uk).

Z. Ding is with the School of Electrical and Electronic Engineering, The University of Manchester, Manchester, UK (e-mail: zhiguo.ding@manchester.ac.uk).

¹In this article, we use “NOMA” to refer to “power-domain NOMA” for simplicity.

ground users can be served. UAVs in coexistence with device-to-device (D2D) communications were studied by the authors of [12], where the user outage probability was analyzed in both static and mobile UAV scenarios. For mobile UAV communication systems, the mobility of UAVs was exploited to further improve the system performance, such as average throughput and secrecy rate. A multiple UAV BSs network was considered by the authors of [13], where the minimum average rate of ground users were maximized by optimizing UAVs' trajectories, transmit power, and user scheduling. The authors of [14] maximized the system secrecy rate by designing UAVs' trajectory and scheduling, where two UAVs were used for information transmission and jamming, respectively. The authors of [15] optimized 3D UAV trajectory in UAV-enabled data harvesting system with Rician fading channel model. Furthermore, a propulsion energy consumption model for rotary-wing UAVs were derived by the authors of [16], where a novel path discretization method was proposed to minimize the energy consumed by the UAV for accomplishing missions. The authors of [17] studied a UAV flight time minimization problem in UAV data collection wireless sensor networks. The authors of [18] minimized the energy consumption of Internet-of-Things (IoT) devices in a UAV-enabled IoT network, subject to the UAV energy constraint. The authors of [19] further studied solar-powered UAV communication systems, where the optimal UAV trajectory and resource allocations were obtained via monotonic optimization.

2) *Studies on UAV-NOMA Systems*: In contrast to the aforementioned research contributions on UAV communication systems considering OMA transmission scheme, some initial studies have focused on UAV-NOMA systems [20–27]. For example, The authors of [21] optimized the UAV attitude as well as power allocation to achieve maximum sum rate when UAV BSs serve ground users employing NOMA. The authors of [22] investigated multiple antennas technique in UAV NOMA communications, where the system performance was analyzed with stochastic geometry approach in both LOS and non-LoS scenarios. The authors of [23] proposed a novel uplink cooperative NOMA framework to tackle the interference introduced by the UAV user. A resource allocation problem was formulated by the authors of [24] in uplink NOMA multi-UAV IoT systems, where the system sum rate was maximized by optimizing subchannel allocation, IoT devices' transmit power, and UAVs' attitude. Furthermore, The authors of [25] maximized the minimum achievable rate of ground users by jointly optimizing the UAV trajectory, transmit power, and user association in the downlink NOMA scenario. A UAV-assisted NOMA network was proposed by The authors of [26], where the UAV trajectory and precoding of the ground base station were jointly designed to maximize the system sum rate. The authors of [27] investigated uplink NOMA with the cellular-connected UAV, where the mission completion time was minimized by designing the UAV trajectory and UAV-BS association order. Moreover, the authors of [28] developed two secure transmission schemes in UAV-NOMA networks for single-user and multiple-user scenarios. The authors of [29] maximized the energy efficiency of mmWave-enabled NOMA-UAV networks by jointly optimizing the deployment location,

hybrid precoding, and power allocation at the UAV.

B. Motivation and Contributions

Despite the aforementioned advantages of UAV data collection systems, one critical issue is that both the on-board energy of UAVs and storage energy of GNs are limited, namely double energy limitations. Therefore, the double energy limitations need to be carefully considered in practical designs to fully reap the benefits of UAV data collection systems. Although some prior works have studied the UAV data collection design [15–18], the energy constraints at either UAV or GNs are often absent and only OMA transmission scheme was employed. To the best of our knowledge, the joint UAV trajectory and resource allocation design under different MA schemes has not been well investigated in the energy-constrained UAV data collection system, especially for NOMA. In contrast to OMA allocating orthogonal resources to different GNs, NOMA introduces additional decoding order design by multiplexing GNs in the same time/frequency resources, which makes the achievable data collection rate from GNs to the UAV more complicated and leads to a more challenging problem than OMA.

Against the above discussion, in this article, we investigate energy-constrained UAV data collection systems with two MA schemes, namely OMA and NOMA. Specifically, the UAV flies from the predefined initial location to the final location to harvest data from GNs, under the constraints on the UAV's and GNs' energy limitations. The main contributions are summarized as follows:

- We propose a energy-constrained UAV data collection framework where both OMA and NOMA are employed at the UAV when collecting data from GNs. Based on the proposed framework, we jointly optimize the UAV trajectory, the GNs' transmit power, and the GN scheduling for maximization of the minimum UAV data collection throughput from all GNs, subject to the energy constraints at both the UAV and GNs.
- For OMA, we develop an efficient algorithm by employing alternating optimization (AO) method, where each non-convex subproblem is iteratively solved by applying successive convex approximation (SCA) technique. We demonstrate that the proposed algorithm is guaranteed to converge.
- For NOMA, we propose a penalty-based algorithm for solving the additional mixed integer non-convex decoding order design subproblem, where the relaxed continuous variables are forced to be binaries through iterations.
- Numerical results demonstrate that the max-min throughput obtained by the proposed algorithm significantly outperforms other benchmark schemes. It also shows that NOMA always achieves no worse performance than that of OMA, and the performance gain of NOMA over OMA is noticeable when GNs have sufficient energy.

C. Organization and Notation

The rest of the paper is organized as follows. Section II presents the system model and problem formulation for both

OMA and NOMA. In Section III and Section IV, two efficient AO-based algorithms are developed for OMA and NOMA, respectively. Section V provides numerical results to validate the effectiveness of the proposed designs. Finally, Section VI concludes the paper.

Notation: Scalars are denoted by lower-case letters, vectors are denoted by bold-face lower-case letters. $\mathbb{R}^{M \times 1}$ denotes the space of M -dimensional real-valued vector. For a vector \mathbf{a} , \mathbf{a}^T denotes its transpose, and $\|\mathbf{a}\|$ denotes its Euclidean norm.

II. SYSTEM MODEL AND PROBLEM FORMULATION

A. System Model

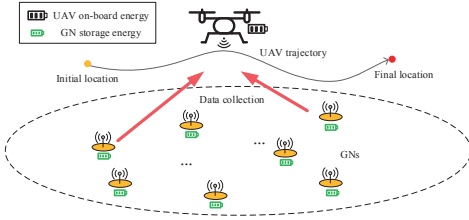


Fig. 1: Illustration of the energy-constrained UAV data collection system.

As shown in Fig. 1, we consider a UAV data collection system, which consists of a rotary-wing single-antenna UAV data collector and K single-antenna GNs. The GNs are indexed by the set $\mathcal{K} = \{1, \dots, K\}$. The UAV is dispatched to fly from the predefined initial location to the final location with a constant height H . During the flight, the UAV collects data from each GN. Without loss of generality, a 3D Cartesian coordinate system is considered. The k th GN is fixed at $(\mathbf{w}_k^T, 0)^T$, where $\mathbf{w}_k = (x_k, y_k)^T$ denotes the corresponding horizontal coordinate. Similarly, $(\mathbf{u}_I^T, H)^T$ and $(\mathbf{u}_F^T, H)^T$ are the UAV's predefined initial and final coordinates, where $\mathbf{u}_I = (x_I, y_I)^T$ and $\mathbf{u}_F = (x_F, y_F)^T$. Let E_U and E_k denote the UAV total on-board energy and the total storage energy of the k th GN, respectively. Let T_U denote the corresponding UAV total flight time, the instant UAV trajectory is denoted by $(\mathbf{u}(t)^T, H)^T$, $0 \leq t \leq T_U$, where $\mathbf{u}(t) \in \mathbb{R}^{2 \times 1}$ is the UAV horizontal location. Different from the existing UAV trajectory design works using the time discretization method [13–15], T_U is unknown and needs to be optimized in our work. To facilitate the design of UAV trajectory, we invoke the path discretization method [16] and divide the UAV path into N line segments with $N + 1$ waypoints, where $\mathbf{u}[1] = \mathbf{u}_I$, $\mathbf{u}[N + 1] = \mathbf{u}_F$. In order to achieve good approximation, we have the following constraints:

$$\|\mathbf{u}[n + 1] - \mathbf{u}[n]\| \leq \delta, n = 1, \dots, N, \quad (1)$$

where δ is chosen sufficiently small compared with the UAV height such that the distance between the UAV and each GN is approximately unchanged and the UAV's speed can be regarded as a constant within each line segment. The time duration of n th line segment is denoted by $T[n]$ and $\sum_{n=1}^N T[n] = T_U$. The constraints introduced by the UAV mobility is given by

$$\|\mathbf{u}[n + 1] - \mathbf{u}[n]\| \leq V_{\max} T[n], n = 1, \dots, N, \quad (2)$$

where V_{\max} denotes the maximum speed of the UAV.

The channel coefficient between the UAV and the k th devices at the n th line segment can be modeled as $h_k[n] = \sqrt{\rho_k[n]} \tilde{h}_k[n]$, where $\rho_k[n]$ represents the distance-dependent large-scale channel attenuation and $\tilde{h}_k[n]$ represents the small-scale fading coefficient. Recent A2G channel modeling literatures [30, 31] have shown that there is a high probability for A2G channel to be dominated by the LoS link, especially for rural or suburban environment², which is also the typical scenario for UAV data collection systems. Therefore, in this paper, we assume that $\tilde{h}_k[n] \triangleq 1$ ³ and the channel coefficient follows from the free-space path loss model, which can be expressed as

$$|h_k[n]|^2 = \frac{\rho_0}{\|\mathbf{u}[n] - \mathbf{w}_k\|^2 + H^2}, \quad (3)$$

where ρ_0 is the channel power gain at the reference distance of 1 meter. It is also assumed that the Doppler effect caused by the UAV mobility is perfectly compensated at the receivers [32].

The energy consumption of UAV involves two parts: the communication related energy and the propulsion energy. Compared with the propulsion energy, the communication related energy is much smaller, and is thus ignored in this paper. Furthermore, we adopt the propulsion power consumption model of rotary-wing UAVs in [16], which is modeled as a function of the UAV's speed and ignores the UAV acceleration/deceleration energy consumption. This model is reasonable when the acceleration/deceleration duration only takes a small portion of the total UAV flight time. Suppose that a rotary-wing UAV flying at the speed of V , the corresponding propulsion power consumption can be calculated as [16]

$$P(V) = P_0 \left(1 + \frac{3V^2}{U_{tip}^2} \right) + P_i \left(\sqrt{1 + \frac{V^4}{4v_0^4} - \frac{V^2}{2v_0^2}} \right)^{1/2} + \frac{1}{2} d_0 \rho s A V^3, \quad (4)$$

where P_0 and P_i are two constants representing the blade profile power and induced power in hovering status, respectively. U_{tip} represents the tip speed of the rotor blade and v_0 represents the mean rotor induced velocity in hover. d_0 and s are the fuselage drag ratio and rotor solidity, respectively. In addition, ρ and A denote the air density and rotor disc area, respectively. During the n th line segment, the UAV speed can be calculated as $V[n] = \frac{s[n]}{T[n]}$, where $s[n] = \|\mathbf{u}[n + 1] - \mathbf{u}[n]\|$. Thus, the

²As reported in [30], a 100% LoS probability A2G channel can be achieved when the height of UAV is larger than 40 m in the rural macro (RMa) scenario.

³In practice, the A2G channel might involve some random parameters, which make the associated optimization problems are complicated to solve. The results in this paper with the deterministic LoS channel model serve as a valuable performance indicator for the considered system, and provide guidelines for practical implementation.

UAV energy consumption at the n th line segment is given by

$$\begin{aligned} E[n] &= T[n] P \left(\frac{s[n]}{T[n]} \right) \\ &= P_0 \left(T[n] + \frac{3s[n]^2}{U_{tip}^2 T[n]} \right) \\ &\quad + P_i \left(\sqrt{T[n]^4 + \frac{s[n]^4}{4v_0^4}} - \frac{s[n]^2}{2v_0^2} \right)^{\frac{1}{2}} + \frac{1}{2} d_0 \rho s A \frac{s[n]^3}{T[n]^2}. \end{aligned} \quad (5)$$

Then, the total UAV energy constraint can be expressed as $\sum_{n=1}^N E[n] \leq E_U$.

The sleep-wake protocol is considered when the UAV collects data from GNs, as assumed in [15, 18]. GNs upload information only when being waken up by the UAV, otherwise they keep in silence. In this paper, an offline design is considered, i.e., first determining the UAV trajectory and the wake-up time allocation scheme using the prior knowledge of GNs' locations and their LoS channel coefficients. Based on the obtained results, during the realistic flight, the UAV wakes up the corresponding GN⁴ at the predefined time instant and location using the wake-up signal [33] and informs them to upload data through the downlink reliable control links. We ignore the energy consumed by the UAV for sending wake-up signal, since it belongs to the communication related energy. In the next subsection, we formulate the optimization problem with two MA schemes, i.e., OMA and NOMA.

B. Problem Formulation for OMA

For OMA, the UAV receives the information bits from different GNs by allocating unique time resources⁵ at each time duration $T[n]$. Let $\tau_k[n]$ denote the allocated time resources for the k th GN during $T[n]$ and we have $\sum_{k=1}^K \tau_k[n] \leq T[n], \forall n$. Recall that the distance between the UAV and each GN is approximately unchanged within each line segment by employing the path discretization method. Therefore, the achievable data collection throughput (bits/Hz) from the k th GN during the n th line segment for OMA is approximate to a constant, which is given by

$$r_k^O[n] = \tau_k[n] \log_2 \left(1 + \frac{\gamma_0 p_k[n]}{\|\mathbf{u}[n] - \mathbf{w}_k\|^2 + H^2} \right), \quad (6)$$

where $\gamma_0 = \frac{\rho_0}{\sigma^2}$ and $p_k[n]$ denotes the transmit power of the k th GN. Therefore, the total achievable throughput from the k th GN during the UAV flight is $Q_k^O = \sum_{n=1}^N r_k^O[n]$. In our work, the circuit power consumptions of GNs are ignored, the total storage energy constraint of the k th GN for OMA is given by $\sum_{n=1}^N \tau_k[n] p_k[n] \leq E_k, \forall k$.

In order to achieve a fair data collection from all GNs, we aim to maximize the minimum UAV data collection throughput

⁴In terms of the wake-up protocol [33], GNs remain in power save state instead of completely off state. As a result, the start time is relatively short and can be ignored as compared with the data uploading duration.

⁵We adopt time division multiple access (TDMA) instead of frequency division multiple access (FDMA) for OMA, since TDMA is more energy-saving and easier for implementation than FDMA in the considered network of this paper.

by jointly optimizing the UAV trajectory, $\{\mathbf{u}[n], T[n]\}$, the GN scheduling, $\{\tau_k[n]\}$, and the GN transmit power, $\{p_k[n]\}$, while taking the energy constraints of both the UAV and GNs into account. Then, the optimization problem for OMA can be formulated as

$$\begin{aligned} & \max_{\{\mathbf{u}[n], T[n], \tau_k[n], p_k[n]\}} \min_{\forall k} Q_k^O & (7a) \\ \text{s.t. } & \mathbf{u}[1] = \mathbf{u}_I, \mathbf{u}[N] = \mathbf{u}_F, & (7b) \\ & \|\mathbf{u}[n+1] - \mathbf{u}[n]\| \leq \min(\delta, V_{\max} T[n]), \forall n, & (7c) \\ & \sum_{n=1}^N E[n] \leq E_U, & (7d) \\ & \sum_{n=1}^N \tau_k[n] p_k[n] \leq E_k, \forall k, & (7e) \\ & \sum_{k=1}^K \tau_k[n] \leq T[n], \forall n, & (7f) \\ & \tau_k[n] \geq 0, \forall k, n, & (7g) \\ & 0 \leq p_k[n] \leq P_{\max}, \forall n, k, & (7h) \end{aligned}$$

where P_{\max} represents the maximum transmit power of GNs. (7b) and (7c) represent the UAV mobility constraints. (7d) and (7e) are energy constraints of the UAV and GNs, respectively.

Remark 1. In Problem (7), time resources are allocated in an adaptive manner. We refer to this type of OMA as OMA-II scheme. However, in conventional OMA, time resources are equally allocated to each GN, which is referred to OMA-I scheme [34]. For OMA-I, Problem (7) needs to consider additional constraints, $\tau_k[n] = \tau_j[n], \forall k \neq j$.

C. Problem Formulation for NOMA

For NOMA, the UAV receives all GNs' signals through the same time resources. Different from the downlink NOMA communication [25], where the SIC decoding order is determined by the channel gains. In uplink NOMA, the UAV can perform SIC in any arbitrary order since all received signals at the UAV are desired signals. Let $\pi_n(k)$ denote the decoding order of GN k at the n th line segment. If $\pi_n(k) = i$, then GN k is the i th signal to be decoded at the n th line segment. Therefore, a set of binary indicators $\alpha_{k,m}[n] \in \{0, 1\}, \forall k \neq m \in \mathcal{K}$ are defined as

$$\alpha_{k,m}[n] = 1, \pi_n(k) > \pi_n(m), \quad (8)$$

$$\alpha_{k,m}[n] + \alpha_{m,k}[n] = 1. \quad (9)$$

Equation (9) ensures that there is only one GN at each decoding order.

Similarly, the UAV received signal-to-interference-plus-noise (SINR) from the k th GN during the n th line segment can be approximate to a constant, which is given by

$$\begin{aligned} \gamma_k^N[n] &= \frac{\gamma_0 p_k[n] |h_k[n]|^2}{\sum_{m \in \mathcal{K}, m \neq k} \alpha_{m,k}[n] \gamma_0 p_m[n] |h_m[n]|^2 + 1} \\ &= \frac{\gamma_0 p_k[n]}{\sum_{m \in \mathcal{K}, m \neq k} \alpha_{m,k}[n] \gamma_0 p_m[n]} \frac{|h_k[n]|^2}{\left(\|\mathbf{u}[n] - \mathbf{w}_k\|^2 + H^2 \right)} \\ &= \frac{\gamma_0 p_k[n]}{\sum_{m \in \mathcal{K}, m \neq k} \alpha_{m,k}[n] \gamma_0 p_m[n]} \frac{|h_k[n]|^2}{\left(\|\mathbf{u}[n] - \mathbf{w}_k\|^2 + H^2 \right) + 1}. \end{aligned} \quad (10)$$

Let $\tau[n]$ denote the UAV allocated time resources for all GNs at the n th line segment, where $\tau[n] \leq T[n], \forall n$. Similarly,

the total data collection throughput from the k th GN during the UAV flight for NOMA is given by

$$Q_k^N = \sum_{n=1}^N r_k^N [n] = \sum_{n=1}^N \tau [n] \log_2 (1 + \gamma_k^N [n]). \quad (11)$$

Moreover, the GNs' energy constraints for NOMA are given by $\sum_{n=1}^N \tau [n] p_k [n] \leq E_k, \forall k$.

By jointly optimizing the UAV trajectory, $\{\mathbf{u} [n], T [n]\}$, the communication time allocation, $\{\tau [n]\}$, the GN transmit power, $\{p_k [n]\}$, and the decoding order, $\{\alpha_{k,m} [n]\}$, the max-min collection throughput optimization problem for NOMA can be formulated as

$$\max_{\{\mathbf{u} [n], T [n], \tau [n], p_k [n], \alpha_{k,m} [n]\}} \min_{\forall k} Q_k^N \quad (12a)$$

$$\text{s.t. } \mathbf{u} [1] = \mathbf{u}_I, \mathbf{u} [N] = \mathbf{u}_F, \quad (12b)$$

$$\|\mathbf{u} [n+1] - \mathbf{u} [n]\| \leq \min(\delta, V_{\max} T [n]), \forall n, \quad (12c)$$

$$\sum_{n=1}^N E [n] \leq E_U, \quad (12d)$$

$$\sum_{n=1}^N \tau [n] p_k [n] \leq E_k, \forall k, \quad (12e)$$

$$0 \leq \tau [n] \leq T [n], \forall n, \quad (12f)$$

$$0 \leq p_k [n] \leq P_{\max}, \forall n, k, \quad (12g)$$

$$\alpha_{k,m} [n] + \alpha_{m,k} [n] = 1, \forall k \neq m \in \mathcal{K}, \quad (12h)$$

$$\alpha_{k,m} [n] \in \{0, 1\}, \forall k, m \in \mathcal{K}, \quad (12i)$$

Problems (7) and (12) are non-convex problems due to the non-convex objective function and constraints, where optimization variables are highly-coupled. Moreover, the introduced binary variables for NOMA decoding orders make (12) become a mixed integer non-convex optimization problem, which is more challenging to solve. Note that there is no standard method to efficiently obtain the globally optimal solution for such problems. In the following, we develop efficient algorithms to find a high-quality suboptimal solution with a polynomial time complexity, by employing AO method and SCA technique.

III. PROPOSED SOLUTION FOR OMA

To make Problem (7) tractable, we first introduce auxiliary variables $\{\theta_k [n], \forall n, k\}$ and $\{\omega [n] \geq 0, \forall n\}$ such that

$$\theta_k [n]^2 = \tau_k [n] B \log_2 \left(1 + \frac{\gamma_0 p_k [n]}{\|\mathbf{u} [n] - \mathbf{w}_k\|^2 + H^2} \right), \quad (13)$$

$$\omega [n] = \left(\sqrt{T [n]^4 + \frac{s [n]^4}{4v_0^4}} - \frac{s [n]^2}{2v_0^2} \right)^{\frac{1}{2}}. \quad (14)$$

Moreover, equation (14) is equivalent to

$$\frac{T [n]^4}{\omega [n]^2} = \omega [n]^2 + \frac{s [n]^2}{v_0^2}. \quad (15)$$

With the above introduced variables and define $\eta^O = \min_{\forall k} Q_k^O$, Problem (7) can be rewritten as the following problem:

$$\max_{\eta^O, \{\mathbf{u} [n], T [n], \tau_k [n], p_k [n], \theta_k [n], \omega [n]\}} \eta^O \quad (16a)$$

$$\text{s.t. } \sum_{n=1}^N \theta_k [n]^2 \geq \eta^O, \forall k, \quad (16b)$$

$$\frac{\theta_k [n]^2}{\tau_k [n]} \leq \log_2 \left(1 + \frac{\gamma_0 p_k [n]}{\|\mathbf{u} [n] - \mathbf{w}_k\|^2 + H^2} \right), \forall n, k, \quad (16c)$$

$$P_0 \sum_{n=1}^N \left(T [n] + \frac{3s [n]^2}{U_{tip}^2 T [n]} \right) + P_i \sum_{n=1}^N \omega [n] + \frac{1}{2} d_0 \rho_s A \sum_{n=1}^N \frac{s [n]^3}{t [n]^2} \leq E_U, \quad (16d)$$

$$\frac{T [n]^4}{\omega [n]^2} \leq \omega [n]^2 + \frac{\|\mathbf{u} [n+1] - \mathbf{u} [n]\|^2}{v_0^2}, \forall n, \quad (16e)$$

$$(7b), (7c), (7e) - (7h). \quad (16f)$$

Proposition 1. Problems (16) and (7) are equivalent.

Proof. Without loss of optimality to Problem (16), constraints (16c) and (16e) can be met with equality. Specifically, assume that if any of constraints in (16c) is satisfied with strict inequality, then we can always increase the corresponding value of $\theta_k [n]^2$ to make the constraint (16c) satisfied with equality without decreasing the objective value. Furthermore, suppose that (16e) are satisfied with strict inequality, we can always reduce the corresponding value of $\omega [n]$ to make the constraint (16e) satisfied with equality with other variables fixed, and at the same time make the constraint (16d) still satisfied without changing the objective value of (16). Therefore, Problems (16) and (7) are equivalent. \square

Based on **Proposition 1**, we only need to focus on how to solve Problem (16). As the first and third terms in (16d) are the perspective of the convex quadratic function and the convex cubic function on the set of real numbers, they are also joint convex functions with respect to $s [n]$ and $T [n]$ since the perspective operation preserves convexity [36, Page 89]. As a result, (16d) is a convex constraint. However, constraints (7e), (16b), (16c), and (16e) are still non-convex, where the optimization variables are high-coupled. To handle this obstacle, in the following, we propose AO-based algorithm. Specifically, the original problem (16) is decomposed into two subproblems, i.e., optimization with fixed transmit power and optimization with fixed UAV locations, which are handled by employing SCA. The two subproblems are alternatingly solved until convergence.

A. Optimization with Fixed Transmit Power

For any given feasible GN transmit power, $\{p_k [n]\}$, the optimization problem can be written as

$$\max_{\eta^O, \{\mathbf{u} [n], T [n], \tau_k [n], \theta_k [n], \omega [n]\}} \eta^O \quad (17a)$$

$$\text{s.t. } (7b), (7c), (7e) - (7f), (16b) - (16e). \quad (17b)$$

Problem (17) is still a non-convex problem due to the non-convex constraints (16b), (16c), and (16e). Fortunately, those non-convex constraints can be handled by utilizing SCA technique. Specifically, to tackle the non-convex constraint (16b), the left hand side (LHS) is a convex function with respect to $\theta_k [n]$. Since any convex functions are lower bounded by their

first-order Taylor expansion, the lower bound of $\theta_k[n]^2$ at a given local point $\theta_k^l[n]$ can be expressed as

$$\theta_k[n]^2 \geq \theta_k^l[n]^2 + 2\theta_k^l[n] (\theta_k[n] - \theta_k^l[n]). \quad (18)$$

For the non-convex constraint (16c), the LHS is jointly convex with respect to $\theta_k[n]$ and $\tau_k[n]$. Though the right hand side (RHS) is not concave with respect to $\mathbf{u}[n]$, it is a convex function with respect to $\|\mathbf{u}[n] - \mathbf{w}_k\|^2$. With given local points $\{\mathbf{u}^l[n]\}$, the lower bound for the RHS of (16c) can be expressed as

$$\begin{aligned} & \log_2 \left(1 + \frac{\gamma_0 p_k[n]}{\|\mathbf{u}[n] - \mathbf{w}_k\|^2 + H^2} \right) \geq R_k^{lb}[n] \\ & = \log_2 \left(1 + \frac{\gamma_0 p_k[n]}{\|\mathbf{u}^l[n] - \mathbf{w}_k\|^2 + H^2} \right) \\ & \quad - \varphi_k^l[n] \left(\|\mathbf{u}[n] - \mathbf{w}_k\|^2 - \|\mathbf{u}^l[n] - \mathbf{w}_k\|^2 \right), \end{aligned} \quad (19)$$

where $\varphi_k^l[n] = \frac{(\log_2 e) \gamma_0 p_k[n]}{(\|\mathbf{u}^l[n] - \mathbf{w}_k\|^2 + H^2)(\|\mathbf{u}^l[n] - \mathbf{w}_k\|^2 + H^2 + \gamma_0 p_k[n])}$.

Similarly, to deal with the non-convex constraint (16e), the RHS is the sum of two convex functions and the lower bound is given by

$$\omega[n]^2 + \frac{\|\mathbf{u}[n+1] - \mathbf{u}[n]\|^2}{v_0^2} \geq \beta^{lb}[n], \quad (20)$$

where

$$\begin{aligned} \beta^{lb}[n] & = \omega^l[n]^2 + \omega^l[n] (\omega[n] - \omega^l[n]) - \frac{\|\mathbf{u}^l[n+1] - \mathbf{u}^l[n]\|^2}{v_0^2} \\ & \quad + \frac{2}{v_0^2} (\mathbf{u}^l[n+1] - \mathbf{u}^l[n])^T (\mathbf{u}[n+1] - \mathbf{u}[n]). \end{aligned}$$

By applying (18)-(20), Problem (17) is approximated as the following optimization problem:

$$\max_{\eta^0, \{\mathbf{u}[n], T[n], \tau_k[n], \theta_k[n], \omega[n]\}} \eta^0 \quad (21a)$$

$$\text{s.t.} \quad \sum_{n=1}^N \left(\theta_k^l[n]^2 + 2\theta_k^l[n] (\theta_k[n] - \theta_k^l[n]) \right) \geq \eta^0, \forall k, \quad (21b)$$

$$\frac{\theta_k[n]^2}{\tau_k[n]} \leq R_k^{lb}[n], \forall k, n, \quad (21c)$$

$$\frac{T[n]^4}{\omega[n]^2} \leq \beta^{lb}[n], \forall n, \quad (21d)$$

$$(7b), (7c), (7e) - (7f), (16d). \quad (21e)$$

Now, (21b) is a linear constraint, and (21c) and (21d) are all convex constraints. Therefore, Problem (21) is a convex problem, which can be efficiently solved by standard convex optimization solvers such as CVX [35]. Due to the adoption of the lower bounds in (18)-(20), any feasible solution of Problem (21) must be also feasible for Problem (17), but the reverse does not hold in general. This means the feasible set of problem (21) is a smaller convex set reduced from the original non-convex feasible set of problem (17). Therefore, the obtained objective value of Problem (21) in general provides a lower bound of that of Problem (17).

B. Optimization with Fixed UAV Locations

Before solving this subproblem, we introduce additional auxiliary variables $\{\varepsilon_k[n], \forall n, k\}$ such that

$$\varepsilon_k[n]^2 = \tau_k[n] p_k[n], \forall n, k. \quad (22)$$

Thus, constraint (7e) can be equivalently expressed as the following two constraints:

$$\sum_{n=1}^N \varepsilon_k[n]^2 \leq E_k, \forall k, \quad (23)$$

$$p_k[n] \leq \frac{\varepsilon_k[n]^2}{\tau_k[n]}, \forall n, k. \quad (24)$$

For any given feasible UAV location, $\{\mathbf{u}[n]\}$, Problem (16) can be written as the following optimization problem:

$$\max_{\eta^0, \{T[n], \tau_k[n], p_k[n], \theta_k[n], \omega[n], \varepsilon_k[n]\}} \eta^0 \quad (25a)$$

$$\text{s.t.} \quad (7f) - (7h), (16b) - (16e), (23), (24). \quad (25b)$$

Now, constraint (16c) is convex since the RHS is a concave function with respect to $p_k[n]$. However, Problem (25) is still a non-convex problem due to the non-convex constraints (16b), (16e), and (24). As described in the previous subsection, we have already introduced how to deal with non-convex constraints (16b) and (16e) with their lower bounds based on the first-order Taylor expansion. Therefore, we only need to concentrate on how to deal with the non-convex constraint (24). Similarly, the RHS of (24) is jointly convex with respect to $\varepsilon_k[n]$ and $\tau_k[n]$. The lower bound with given local points $\{\varepsilon_k^l[n], \tau_k^l[n]\}$ can be expressed as

$$\begin{aligned} \frac{\varepsilon_k[n]^2}{\tau_k[n]} & \geq \chi_k^{lb}[n] = \frac{\varepsilon_k^l[n]^2}{\tau_k^l[n]} + \frac{2\varepsilon_k^l[n]}{\tau_k^l[n]} (\varepsilon_k[n] - \varepsilon_k^l[n]) \\ & \quad - \frac{\varepsilon_k^l[n]^2}{\tau_k^l[n]^2} (\tau_k[n] - \tau_k^l[n]), \forall n, k, \end{aligned} \quad (26)$$

By replacing these non-convex constraints with their lower bounds, Problem (25) can be written as the following approximate optimization problem:

$$\max_{\eta^0, \{T[n], \tau_k[n], p_k[n], \theta_k[n], \omega[n], \varepsilon_k[n]\}} \eta^0 \quad (27a)$$

$$\text{s.t.} \quad \sum_{n=1}^N \left(\theta_k^l[n]^2 + 2\theta_k^l[n] (\theta_k[n] - \theta_k^l[n]) \right) \geq \eta^0, \forall k, \quad (27b)$$

$$p_k[n] \leq \chi_k^{lb}[n], \forall n, k, \quad (27c)$$

$$\frac{T[n]^4}{\omega[n]^2} \leq \omega^l[n]^2 + 2\omega^l[n] (\omega[n] - \omega^l[n]) + \frac{s[n]^2}{v_0^2}, \forall n, \quad (27d)$$

$$(7f) - (7h), (16c), (16d), (23). \quad (27e)$$

It can be verified that Problem (27) is a convex problem, which can be efficiently solved by standard convex optimization solvers such as CVX [35]. Similarly, the obtained objective value obtained from Problem (27) serves a lower bound of that of Problem (25) owing to the replacement of non-convex terms with their lower bounds.

C. Overall Algorithm, Complexity, and Convergence

Based on the two subproblems in the previous subsections, we propose an efficient algorithm to solve Problem (16) by invoking AO method. Specifically, Problems (21) and (27) are alternately solved. The obtained solutions in each iteration are used as the input local points for the next iteration. The details of the proposed algorithm for OMA are summarized in **Algorithm 1**. The complexity of each subproblem with interior-point method are $\mathcal{O}\left((3N + 2NK)^{3.5}\right)$ and $\mathcal{O}\left((2N + 4NK)^{3.5}\right)$. Then, the total complexity for OMA is $\mathcal{O}\left(N_{\text{ite}}^{\text{O}}\left((5N + 6NK)^{3.5}\right)\right)$, where $N_{\text{ite}}^{\text{O}}$ denotes the number of iterations needed for the convergence of **Algorithm 1** [36]. It can be observed that the complexity of **Algorithm 1** is polynomial⁶.

Remark 2. Although **Algorithm 1** is designed for solving the optimization problem with OMA-II, it is also applied for OMA-I with linear constraints: $\tau_k[n] = \tau_j[n], \forall k \neq j$.

Next, we demonstrate the convergence of **Algorithm 1**. The objective value of Problem (16) in the l th iteration is defined as $\eta^{\text{O}}(\{\mathbf{u}^l[n]\}, \{T^l[n]\}, \{\tau_k^l[n]\}, \{p_k^l[n]\})$. First, for Problem (21) with given transmit power in step 2 of **Algorithm 1**, we have

$$\begin{aligned} & \eta^{\text{O}}(\{\mathbf{u}^l[n]\}, \{T^l[n]\}, \{\tau_k^l[n]\}, \{p_k^l[n]\}) \\ & \stackrel{(a)}{=} \eta_p^{\text{lb}}(\{\mathbf{u}^l[n]\}, \{T^l[n]\}, \{\tau_k^l[n]\}, \{p_k^l[n]\}) \\ & \stackrel{(b)}{\leq} \eta_p^{\text{lb}}(\{\mathbf{u}^{l+1}[n]\}, \{T^{l+0.5}[n]\}, \{\tau_k^{l+0.5}[n]\}, \{p_k^l[n]\}) \\ & \stackrel{(c)}{\leq} \eta^{\text{O}}(\{\mathbf{u}^{l+1}[n]\}, \{T^{l+0.5}[n]\}, \{\tau_k^{l+0.5}[n]\}, \{p_k^l[n]\}), \end{aligned} \quad (28)$$

where η_p^{lb} represents the objective value of Problem (21) with fixed transmit power. (a) follows the fact that the first-order Taylor expansions are tight at the given local points in Problem (21); (b) holds since Problem (21) is solved optimally; (c) holds due to the fact that the objective value of Problem (21) serves the lower bound of that of (17). The inequality in (28) suggests that the objective value of the original Problem (17) is still non-decreasing after each iteration even if we only solve the approximate Problem (21).

Similarly, for Problem (27) with given UAV location in step 3 of **Algorithm 1**, we have

$$\begin{aligned} & \eta^{\text{O}}(\{\mathbf{u}^{l+1}[n]\}, \{T^{l+0.5}[n]\}, \{\tau_k^{l+0.5}[n]\}, \{p_k^l[n]\}) \\ & = \eta_{\mathbf{u}}^{\text{lb}}(\{\mathbf{u}^{l+1}[n]\}, \{T^{l+0.5}[n]\}, \{\tau_k^{l+0.5}[n]\}, \{p_k^l[n]\}) \\ & \leq \eta_{\mathbf{u}}^{\text{lb}}(\{\mathbf{u}^{l+1}[n]\}, \{T^{l+1}[n]\}, \{\tau_k^{l+1}[n]\}, \{p_k^{l+1}[n]\}) \\ & \leq \eta^{\text{O}}(\{\mathbf{u}^{l+1}[n]\}, \{T^{l+1}[n]\}, \{\tau_k^{l+1}[n]\}, \{p_k^{l+1}[n]\}), \end{aligned} \quad (29)$$

where $\eta_{\mathbf{u}}^{\text{lb}}$ represents the objective value of Problem (27) with fixed UAV location.

⁶Note that the proposed algorithm is still applicable to the case with a large number of GNs. This is because we consider an offline design and **Algorithm 1** is applied prior to the realistic UAV flight. Therefore, the potentially high complexity caused by large K is acceptable given the available computing power.

Algorithm 1 Proposed AO-based Algorithm for Solving Problem (16)

Initialize feasible solutions $\{\mathbf{u}^0[n], T^0[n], \tau_k^0[n], p_k^0[n]\}$ to (16), $l = 0$.

1: **repeat**

2: Solve Problem (21) for given $\{p_k^l[n]\}$, and denote the optimal solutions as $\{\mathbf{u}^{l+1}[n], T^{l+0.5}[n], \tau_k^{l+0.5}[n]\}$.

3: Solve Problem (27) for given $\{\mathbf{u}^{l+1}[n]\}$, and denote the optimal solutions as $\{p_k^{l+1}[n], T^{l+1}[n], \tau_k^{l+1}[n]\}$.

4: $l = l + 1$.

5: **until** the fractional increase of the objective value is below a threshold $\xi > 0$.

As a result, based on (28) and (29), we obtain that

$$\begin{aligned} & \eta^{\text{O}}(\{\mathbf{u}^l[n]\}, \{T^l[n]\}, \{\tau_k^l[n]\}, \{p_k^l[n]\}) \\ & \leq \eta^{\text{O}}(\{\mathbf{u}^{l+1}[n]\}, \{T^{l+1}[n]\}, \{\tau_k^{l+1}[n]\}, \{p_k^{l+1}[n]\}). \end{aligned} \quad (30)$$

Equation (30) means the objective value of Problem (16) is non-decreasing after each iteration. Since the max-min UAV data collection throughput is upper bounded by a finite value due to the limited energy at the UAV and GNs, the proposed algorithm is guaranteed to converge.

IV. PROPOSED SOLUTION FOR NOMA

To solve the formulated optimization problem for NOMA, we can use the same method to tackle the non-convex UAV energy constraint by introducing auxiliary variables $\{\omega[n] \geq 0\}$, as described in the previous section. To deal with other non-convexities of Problem (12), we first introduce auxiliary variables $\{S_k[n]\}, \{I_k[n]\}, \{d_k[n]\}$, and $\{\theta_k[n]\}$ such that

$$S_k[n] = \frac{\|\mathbf{u}[n] - \mathbf{w}_k\|^2 + H^2}{\gamma_0 p_k[n]}, \forall k, n, \quad (31)$$

$$I_k[n] = \sum_{m \in \mathcal{K}, m \neq k} \gamma_0 \alpha_{m,k}[n] p_m[n] d_m[n]^{-1} + 1, \forall k, n, \quad (32)$$

$$d_k[n] = \|\mathbf{u}[n] - \mathbf{w}_k\|^2 + H^2, \forall k, n, \quad (33)$$

$$\theta_k[n]^2 = \tau[n] B \log_2 \left(1 + \frac{1}{S_k[n] I_k[n]} \right), \forall k, n. \quad (34)$$

Define $\eta^{\text{N}} = \min_{\forall k} Q_k^{\text{N}}$, Problem (12) can be equivalently rewritten as

$$\max_{\eta^{\text{N}}, \{S_k[n], I_k[n], \theta_k[n], \omega[n], d_k[n]\}} \eta^{\text{N}} \quad (35a)$$

$$\text{s.t.} \quad \sum_{n=1}^N \theta_k[n]^2 \geq \eta^{\text{N}}, \forall k, \quad (35b)$$

$$\frac{\theta_k[n]^2}{\tau[n]} \leq \log_2 \left(1 + \frac{1}{S_k[n] I_k[n]} \right), \forall k, n, \quad (35c)$$

$$S_k[n] \geq \frac{\|\mathbf{u}[n] - \mathbf{w}_k\|^2 + H^2}{\gamma_0 p_k[n]}, \forall k, n, \quad (35d)$$

$$\begin{aligned} & I_k[n] \geq \\ & \sum_{m \in \mathcal{K}, m \neq k} \gamma_0 \alpha_{m,k}[n] p_m[n] d_m[n]^{-1} + 1, \forall k, n, \end{aligned} \quad (35e)$$

$$d_k[n] \leq \|\mathbf{u}[n] - \mathbf{w}_k\|^2 + H^2, \forall k, n, \quad (35f)$$

$$P_0 \sum_{n=1}^N \left(T[n] + \frac{3s[n]^2}{U_{tip}^2 T[n]} \right) + P_i \sum_{n=1}^N \omega[n] + \frac{1}{2} d_0 \rho s A \sum_{n=1}^N \frac{s[n]^3}{t[n]^2} \leq EU, \quad (35g)$$

$$\frac{T[n]^4}{\omega[n]^2} \leq \omega[n]^2 + \frac{\|\mathbf{u}[n+1] - \mathbf{u}[n]\|^2}{v_0^2}, \forall n, \quad (35h)$$

$$(12b), (12c), (12e) - (12i). \quad (35i)$$

The equivalence between (12) and (35) can be shown similarly as **Proposition 1**. It is observed that Problem (35) has a similar structure with Problem (16) except integer constraints. Therefore, we still decompose (35) into several subproblems, which are ease to handle.

A. Optimization with Fixed Transmit Power and Decoding Order

For any given feasible GN transmit power, $\{p_k[n]\}$, and decoding orders, $\{a_{k,m}[n]\}$, the optimization problem can be written as

$$\max_{\eta^N, \left\{ \mathbf{u}[n], T[n], \tau[n], S_k[n], I_k[n], \theta_k[n], \omega[n], d_k[n] \right\}} \eta^N \quad (36a)$$

$$\text{s.t. } (12b), (12c), (12e), (12f), (35b) - (35h). \quad (36b)$$

Problem (36) is still non-convex owing to the non-convex constraints (35b), (35c), (35f), and (35h). Specifically, (35b) and (35h) can be handled as introduced in the previous section. Before handling the non-convex constraint (35c), we first have the following lemma.

Lemma 1. For $x > 0$ and $y > 0$, $f(x, y) = \log_2 \left(1 + \frac{1}{xy} \right)$ is a joint convex function with respect to x and y

Proof. Lemma 1 can be proved by showing the Hessian matrix of function $f(x, y)$ is positive semidefinite when $x > 0$ and $y > 0$. As a result, $f(x, y)$ is a convex function. \square

Based on **Lemma 1**, the RHS of (35c) is jointly convex with respect to $S_k[n]$ and $I_k[n]$. Thus, by applying the first-order Taylor explanation, the lower bound at given local points $\{S_k^l[n], I_k^l[n]\}$ can be expressed as

$$\log_2 \left(1 + \frac{1}{S_k[n] I_k[n]} \right) \geq R_k^{lb}[n] = \log_2 \left(1 + \frac{1}{S_k^l[n] I_k^l[n]} \right) - \frac{(\log_2 e) (S_k[n] - S_k^l[n])}{S_k^l[n] + S_k^l[n]^2 I_k^l[n]} - \frac{(\log_2 e) (I_k[n] - I_k^l[n])}{I_k^l[n] + I_k^l[n]^2 S_k^l[n]}. \quad (37)$$

Furthermore, for the non-convex constraints (35f), the RHS is a convex function with respect to $\mathbf{u}[n]$. The corresponding lower bound at given local points $\mathbf{u}^l[n]$ is expressed as

$$\|\mathbf{u}[n] - \mathbf{w}_k\|^2 \geq \|\mathbf{u}^l[n] - \mathbf{w}_k\|^2 + 2(\mathbf{u}^l[n] - \mathbf{w}_k)^T (\mathbf{u}[n] - \mathbf{u}^l[n]). \quad (38)$$

Therefore, Problem (36) is approximated as the following optimization problem:

$$\max_{\eta^N, \left\{ \mathbf{u}[n], T[n], \tau[n], S_k[n], I_k[n], \theta_k[n], \omega[n], d_k[n] \right\}} \eta^N \quad (39a)$$

$$\text{s.t. } \sum_{n=1}^N \left(\theta_k^l[n]^2 + 2\theta_k^l[n] (\theta_k[n] - \theta_k^l[n]) \right) \geq \eta^N, \forall k, \quad (39b)$$

$$\frac{\theta_k[n]^2}{\tau_k[n]} \leq R_k^{lb}[n], \forall k, n, \quad (39c)$$

$$d_k[n] \leq H^2 + \|\mathbf{u}^l[n] - \mathbf{w}_k\|^2 + 2(\mathbf{u}^l[n] - \mathbf{w}_k)^T (\mathbf{u}[n] - \mathbf{u}^l[n]), \quad (39d)$$

$$\frac{T[n]^4}{\omega[n]^2} \leq \beta^{lb}[n], \forall n, \quad (39e)$$

$$(12b), (12c), (12e), (12f), (35d), (35e), (35g). \quad (39f)$$

Problem (39) is a convex problem that can be efficiently solved by standard convex optimization solvers such as CVX [35]. The optimal objective value obtained from Problem (39) provides a lower bound to that of Problem (36).

B. Optimization with Fixed UAV Locations and Decoding Order

For any given feasible UAV location $\{\mathbf{u}[n]\}$ and decoding orders $\{a_{k,m}[n]\}$, Problem (35) with auxiliary variables $\{\varepsilon[n]\}$ can be written as the following optimization problem

$$\max_{\eta^N, \left\{ T[n], \tau[n], p_k[n], S_k[n], I_k[n], \theta_k[n], \omega[n], \varepsilon[n], d_k[n] \right\}} \eta^N \quad (40a)$$

$$\text{s.t. } \sum_{n=1}^N \varepsilon_k[n]^2 \leq E_k, \forall k, \quad (40b)$$

$$p_k[n] \leq \frac{\varepsilon_k[n]^2}{\tau[n]}, \forall n, k, \quad (40c)$$

$$(12f), (12g), (35b) - (35h). \quad (40d)$$

By replacing those non-convex terms involved in Problem (40) with their lower bounds, (40) is approximated as the following problem

$$\max_{\eta^N, \left\{ T[n], \tau[n], p_k[n], S_k[n], I_k[n], \theta_k[n], \omega[n], \varepsilon[n], d_k[n] \right\}} \eta^N \quad (41a)$$

$$\text{s.t. } \sum_{n=1}^N \left(\theta_k^l[n]^2 + 2\theta_k^l[n] (\theta_k[n] - \theta_k^l[n]) \right) \geq \eta^N, \forall k, \quad (41b)$$

$$\frac{\theta_k[n]^2}{\tau[n]} \leq R_k^{lb}[n], \forall k, n, \quad (41c)$$

$$p_k[n] \leq \chi_k^{lb}[n], \forall n, k, \quad (41d)$$

$$\frac{T[n]^4}{\omega[n]^2} \leq \omega^l[n]^2 + 2\omega^l[n] (\omega[n] - \omega^l[n]) + \frac{s[n]^2}{v_0^2}, \forall n, \quad (41e)$$

$$(12f), (12g), (35d) - (35g). \quad (41f)$$

Here, the expression of $\chi_k^{lb}[n]$ is obtained by dropping the index k of $\tau_k^l[n]$ and $\tau_k[n]$ in (26). Then, Problem (41) is a convex problem that can be efficiently solved by standard

convex optimization solvers such as CVX [35], and the optimal objective value obtained from Problem (41) serves a lower bound of that of Problem (40).

C. Decoding Order Design with Other Variables Fixed

For any given feasible UAV trajectory, $\{\mathbf{u}[n], T[n]\}$, the time allocation, $\{\tau[n]\}$, and the GN transmit power, $\{p_k[n]\}$, the optimization problem (35) is reduced to

$$\max_{\eta^N, \{\alpha_{k,m}[n], I_k[n]\}} \eta^N \quad (42a)$$

$$\text{s.t. } \sum_{n=1}^N \tau[n] \log_2 \left(1 + \frac{1}{S_k[n] I_k[n]} \right) \geq \eta^N, \forall k, \quad (42b)$$

$$(12h), (12i), (35e). \quad (42c)$$

Involving integer constraints (12i) and non-convex constraint (42b), Problem (42) is a mixed integer non-convex optimization problem. The integer constraint (12i) can be equivalently transformed into the following two constraints:

$$\sum_{k=1}^K \sum_{m \neq k}^K (\alpha_{k,m}[n]^2 - \alpha_{k,m}[n]) \geq 0, \quad (43)$$

$$0 \leq \alpha_{k,m}[n] \leq 1, \forall k \neq m \in \mathcal{K}. \quad (44)$$

Consequently, Problem (42) can be reformulated with continuous variables $\{\alpha_{k,m}[n]\}$ as

$$\max_{\eta^N, \{\alpha_{k,m}[n], I_k[n]\}} \eta^N \quad (45a)$$

$$\text{s.t. } (12h), (35e), (42b), (43), (44). \quad (45b)$$

Though removing integer constraints, Problem (45) is still a non-convex problem with non-convex constraints (42b) and (43). Before handling Problem (45), we first have the following theorem.

Theorem 1. For a sufficiently large constant value $\lambda \gg 1$, Problem (45) is equivalent to the following problem

$$\max_{\eta^N, \{\alpha_{k,m}[n], I_k[n]\}} \eta^N + \lambda \sum_{k=1}^K \sum_{m \neq k}^K (\alpha_{k,m}[n]^2 - \alpha_{k,m}[n]) \quad (46a)$$

$$\text{s.t. } (12h), (35e), (42b), (44). \quad (46b)$$

where λ represents a penalty factor to penalize the objective function for any $\alpha_{k,m}[n]$ that is not equal to 0 or 1.

Proof. See Appendix A. \square

To handle Problem (46), we only need to deal with the non-convex objective function (46) and the non-convex constraint (42b). The second term of (46) is a convex function with respect to $\alpha_{k,m}[n]$. By utilizing the first-order Taylor expansion at a given local point $\alpha_{k,m}^l[n]$, the lower bound is expressed as

$$\alpha_{k,m}[n]^2 \geq \xi_{k,m}[n] = \alpha_{k,m}^l[n]^2 + 2\alpha_{k,m}^l[n] (\alpha_{k,m}[n] - \alpha_{k,m}^l[n]). \quad (47)$$

Algorithm 2 Proposed Penalty-based Algorithm for Solving Problem (49)

Initialize the penalty factor λ and feasible solutions $\{\alpha_{k,m}^l[n]\}$ to (46) with given $\{\mathbf{u}[n], T[n], \tau[n], p_k[n]\}$, $l = 0$.

1: **repeat**

2: Solve Problem (49) with $\{\alpha_{k,m}^l[n]\}$, and denote optimal solutions as $\{\alpha_{k,m}^{l+1}[n]\}$.

3: $l = l + 1$.

4: **until** the fractional increase of the objective value is below a threshold $\xi > 0$.

For the non-convex constraint (42b), the LHS is a convex function with respect to $I_k[n]$. Similarly, the lower bound at given local points $\{I_k^l[n]\}$ is expressed as

$$\begin{aligned} \log_2 \left(1 + \frac{1}{S_k[n] I_k[n]} \right) &\geq \mu_k^{lb}[n] \\ &= \log_2 \left(1 + \frac{1}{S_k[n] I_k^l[n]} \right) - \frac{(\log_2 e) (I_k[n] - I_k^l[n])}{I_k^l[n] + S_k[n] I_k^l[n]^2}. \end{aligned} \quad (48)$$

Based on (47) and (48), Problem (46) can be approximated as the following problem:

$$\max_{\eta^N, \{\alpha_{k,m}[n], I_k[n]\}} \eta^N + \lambda \sum_{k=1}^K \sum_{m \neq k}^K (\xi_{k,m}[n] - \alpha_{k,m}[n]) \quad (49a)$$

$$\text{s.t. } \sum_{n=1}^N \tau[n] \mu_k^{lb}[n] \geq \eta^N, \forall k, \quad (49b)$$

$$(12h), (35e), (42b), (44). \quad (49c)$$

Problem (49) is a convex problem that can be solved efficiently by standard convex program solvers such as CVX [35]. Specifically, we develop an iterative algorithm to optimize the decoding orders for given UAV trajectory, time allocation, and transmit power as summarized in **Algorithm 2**. Since the application of lower bounds approximation, the obtained result serves a lower bound of that of Problem (46).

D. Overall Algorithm, Complexity, and Convergence

Based on subproblems in the previous three subsections, we propose an efficient iterative algorithm to solve Problem (12) by invoking AO method. The details of the designed algorithm for NOMA are summarized in **Algorithm 3**. The complexity of each subproblem with interior-point method are $\mathcal{O}((4N + 4NK)^{3.5})$, $\mathcal{O}((4N + 5NK)^{3.5})$, and $\mathcal{O}(N_{\text{ite}}^2 (NK^2 + NK)^{3.5})$, respectively, where N_{ite}^2 is the number of iterations required for the convergence of **Algorithm 2**. Therefore, the total complexity for NOMA is $\mathcal{O}(N_{\text{ite}}^N ((8N + 9NK)^{3.5} + N_{\text{ite}}^2 (NK^2 + NK)^{3.5}))$, where N_{ite}^N is the iteration number of **Algorithm 3** for NOMA [36]. It can be seen that complexity of NOMA is larger than that of OMA. The convergence of **Algorithm 3** can be shown similarly as that of **Algorithm 1**. The details are omitted for brevity.

Algorithm 3 Proposed AO-based Algorithm for Solving Problem (12)

Initialize feasible solutions to (7)

$$\{\mathbf{u}^0[n], T^0[n], \tau^0[n], p_k^0[n], \alpha_{k,m}^0[n]\}. l = 0.$$

 1: **repeat**

 2: Solve Problem (39) for given $\{p_k^l[n], a_{k,m}^l[n]\}$, and denote the optimal solutions by $\{\mathbf{u}^{l+1}[n], T^{l+0.5}[n], \tau^{l+0.5}[n]\}$.

 3: Solve Problem (41) for given $\{\mathbf{u}^{l+1}[n], a_{k,m}^l[n]\}$, and denote the optimal solutions by $\{p_k^{l+1}[n], T^{l+1}[n], \tau^{l+1}[n]\}$.

 4: Solve Problem (49) for given $\{\mathbf{u}^{l+1}[n], T^{l+1}[n], \tau^{l+1}[n], p_k^{l+1}[n]\}$ via **Algorithm 2**. Denote the optimal solutions by $\{\alpha_{k,m}^{l+1}[n]\}$.

 5: $l = l + 1$.

 6: **until** the fractional increase of the objective value is below a threshold $\xi > 0$.

V. NUMERICAL EXAMPLES

In this section, numerical examples are provided to evaluate the performances of the proposed algorithms. In the simulations, we consider a UAV data collection system with $K = 5$ GNs, which are randomly and uniformly distributed in a square area of 500×500 m². As the maximum allowed UAV height in federal aviation authority (FAA) regulations is 122m, the height of the UAV is fixed at $H = 100$ m to make the A2G channel can be well approximated by the LoS channel model. The UAV is assumed to fly from the initial location $(0, 0, 100)^T$ m to the final location $(500, 500, 100)^T$ m. The maximum UAV speed is $V_{\max} = 30$ m/s. For the rotary-wing UAV propulsion power consumption model in (4), we set the parameters as follows⁷ [16]: $P_0 = 79.86$ W, $P_i = 88.63$ W, $U_{tip} = 120$ m/s, $v_0 = 4.03$ m/s, $d_0 = 0.6$, $\rho = 1.225$ kg/m³, $s = 0.05$, $A = 0.503$ m². The received SNR at a reference distance of 1 m is $\gamma_0 = 50$ dB. The maximum transmit power of GNs is set to $P_{\max} = 0.1$ W. As the max-min problem is considered to guarantees the fairness among GNs, without lose of generality, we assume that all GNs have identical storage energy (i.e., $E_k = E_s, \forall k$) to ensure them in a fair initial state. The algorithm threshold ξ is set to 10^{-2} . The following results are obtained based on one random GN deployment as illustrated in Fig. 3 via changing different parameters (e.g., UAV on-board energy and GN storage energy).

In Fig. 2, we first study the convergence of **Algorithm 1** and **Algorithm 3** for OMA and NOMA cases with $E_s = 10$ Joule (J). The initial UAV trajectory, $\{\mathbf{u}^0[n], T^0[n]\}$, is set to the straight flight from the initial location to the final location with the maximum-range (MR) speed in [16]. For OMA, the initial time allocation, $\{\tau_k^0[n]\}$, and initial transmit power, $\{p_k^0[n]\}$, are obtained by letting $\tau_k^0[n] = \frac{T^0[n]}{K}$ and $p_k^0[n] = \min\left(P_{\max}, E_s / \sum_{n=1}^N \tau_k^0[n]\right), \forall k, n$. For NOMA, the initial time allocation, $\{\tau^0[n]\}$, and initial transmit power,

⁷As reported in [Table I, 16], the parameters for the rotary-wing UAV propulsion power consumption model are selected in terms of the physical model of the UAV (e.g., UAV weight, rotor size, blade angular, etc) and the objective environment (i.e., air density).

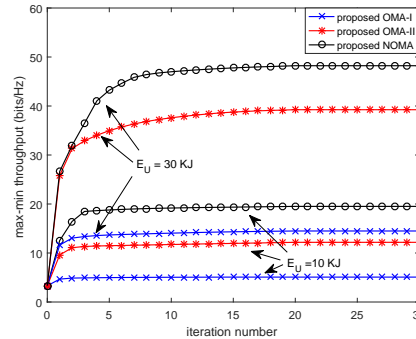
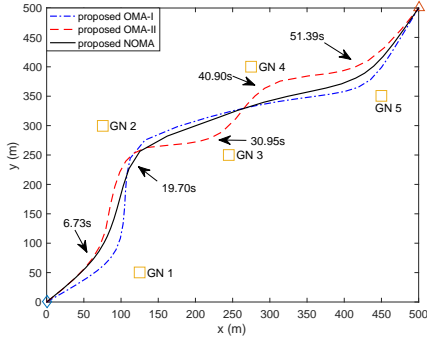
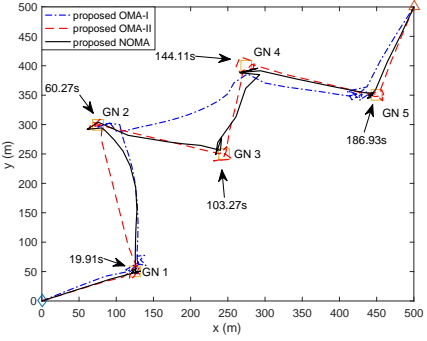


Fig. 2: Convergence of the proposed algorithms.

$\{p_k^0[n]\}$, are obtained by letting $\tau^0[n] = T^0[n]$ and $p_k^0[n] = \min\left(P_{\max}, E_s / \sum_{n=1}^N \tau^0[n]\right), \forall k, n$. We consider two cases with $E_U = 10$ KJ and $E_U = 30$ KJ. From the figure, it is observed that the max-min achievable throughput of three schemes increase as the number of iterations increases. When $E_U = 10$ KJ, the proposed algorithm for three schemes converges with around 10 iterations. When $E_U = 30$ KJ, the proposed algorithm converges with around 25 iterations. The reasons behind this can be explained as follows. Since $E_U = 30$ KJ enables more degrees-of-freedom for UAV trajectory design than $E_U = 10$ KJ, the UAV for large E_U can achieve more complex trajectory to collect more information bits than that for small E_U (which are shown in the following optimize UAV trajectories of Fig. 3). However, recall the fact that the initial UAV trajectory is same for different E_U and the employed path discretization method makes the displacement of the UAV at each iteration is relatively small. Therefore, the proposed algorithm for $E_U = 30$ KJ needs more iterations to converge than that for $E_U = 10$ KJ.

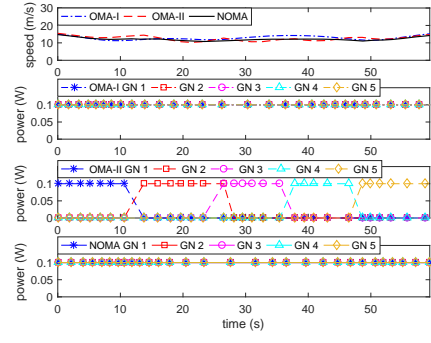
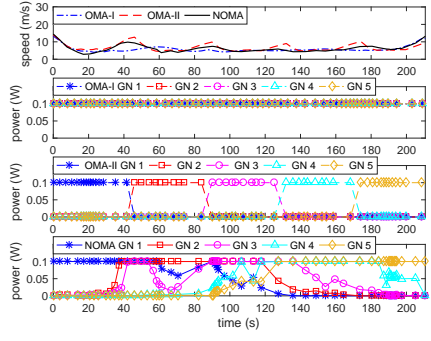
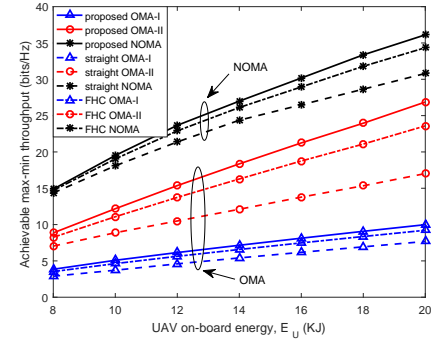
In Fig. 3, we provide the optimized UAV trajectory for different MA schemes with $E_s = 10$ J and different E_U . In order to illustrate the variety of the instant UAV speed and GNs' transmit power shown in Fig. 4, Fig. 3 also presents the time instant when the UAV is closest to each GN in the OMA-II scheme. It is first observed from Fig. 3 that the UAV tries to successively fly as close as possible to each GN in both three schemes even with different E_U . This is expected since the considered max-min throughput objective function makes the UAV need to collect data from each GN in a fair manner. When the UAV on-board energy is small, e.g., $E_U = 8$ KJ, the obtained UAV paths and speeds for three schemes are similar, as shown in Fig. 3(a) and Fig. 4(a). Regarding GNs' transmit power, GNs in all schemes tend to transmit at P_{\max} as long as being waken up by the UAV. This is because, in this case, E_s is large enough compared with the total available communication time. Note that GNs transmit in a successive manner for OMA-II. This is because the optimization of time resources allocation in OMA-II allows the UAV to allocate all the communication time resources to its nearest GN along the trajectory, thus collecting more information bits. This phenomena can be also verified by the time instant in Fig. 3 and the corresponding GN awake state in Fig. 4. Though all GNs transmit at P_{\max} through the whole UAV flight time in NOMA and OMA-I, the reasons

(a) $E_U = 8$ KJ.(b) $E_U = 30$ KJ.Fig. 3: The optimized UAV trajectories for different MA schemes and $E_s = 10$ J.

are different. For NOMA, all GNs are multiplexed in power levels within the same time/frequency resources. As a result, the UAV can not only wake up its nearest GNs but also other GNs to collect more data. However, for OMA-I, as the time resources are always equally allocated to GNs, GNs need to stay awake throughout the whole time to upload more data to the UAV.

In Fig. 3(b) and Fig. 4(b) for $E_U = 30$ KJ, the UAV in general successively flies to the top of each GN in both schemes. It is observed that the UAV keeps flying around at the top of GNs other than remaining static. The reason is that the UAV will consume much higher energy to hover in the air than flying around with a certain speed. Therefore, the saved energy by flying around instead of hovering can prolong the communication time and increase the achieved throughput. Moreover, GNs in NOMA do not always keep awake when $E_U = 30$ KJ. This is expected since the UAV flight time for $E_U = 30$ KJ is rather large, the storage energy E_s is not enough to allow GNs to keep transmitting. As a result, the UAV tends to wake up some of GNs to get full use of the limited energy stored at each GN. For OMA-I with $E_U = 30$ KJ, GNs still keep awake during the UAV flight time due to the equal time allocation. It also causes the UAV for NOMA and OMA-I in Fig. 3(b) flies a curve between two GNs instead of a straight line for OMA-II since the UAV tends to maximize the rate of all awake GNs while flying.

In Fig. 5, we provide the max-min throughput versus the UAV on-board energy E_U with $E_s = 10$ J for different MA schemes. For comparison, we consider the following benchmark schemes:

(a) $E_U = 8$ KJ.(b) $E_U = 30$ KJ.Fig. 4: The optimized speed of the UAV and transmit power of GNs for different MA schemes and $E_s = 10$ J.Fig. 5: Max-min throughput versus the UAV on-board energy of different schemes for $E_s = 10$ J.

- **Straight X**: In this case, the UAV flies from \mathbf{u}_I to \mathbf{u}_F in a straight line. The corresponding max-min achievable throughput is obtained by solving Problems (16) and (35) with additional linear constraints $\mathbf{u}(1, n) = \mathbf{u}(2, n), \forall n$. Meanwhile, X represents different MA schemes, such as OMA-I, OMA-II, and NOMA.
- **FHC X**: In this case, the UAV collects data from GNs following from the fly-hover-communicate (FHC) protocol as did in [16]. The optimization problem becomes to find the optimal hovering locations and the corresponding resource allocations.

As illustrated, it is first observed that the max-min throughput of all considered schemes increases with the increase of E_U since the UAV is able to collect more information bits from GNs with a longer flight time. In particular, the performance gain of the proposed scheme or the FHC scheme over the

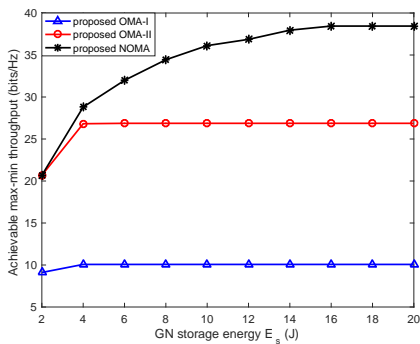


Fig. 6: Max-min throughput versus the GN storage energy with $E_U = 20$ KJ.

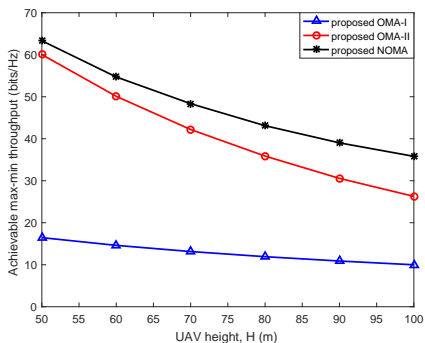


Fig. 7: Max-min throughput versus the UAV height for $E_U = 20$ KJ and $E_s = 10$ J.

scheme with a straight trajectory becomes more pronounced as E_U increases. This is because a larger value of E_U allows the UAV to fly closer to collect data from GNs, which also validates the benefits of UAV trajectory design. It is also observed that the proposed scheme outperforms the FHC scheme. This is expected since the UAV would consume more energy to hover in the air, which reduces the total UAV flight time. Moreover, NOMA achieves a better performance than OMA. The performance gain achieved by NOMA comes from the multiplexing of all GNs in power domain. Note that OMA-I achieves the worst performance since the UAV needs to allocate time resources equally to all GNs, which reduces the throughput of GNs which have good channel conditions (i.e., near from the UAV).

Fig. 6 presents the max-min throughput versus the GN storage energy E_s for different schemes with $E_U = 20$ KJ. From the figure, the max-min throughput of all schemes improves with the increase of E_s at first and remains unchanged. This is because, for a given E_U , the UAV can allocate more time to GNs for uploading information when E_s is limited. The max-min throughput remains unchanged until all the UAV flight time is occupied for GNs uploading data with P_{\max} . In this case, the increase of E_s has no effect on the obtained max-min throughput since the total energy consumption of GNs is fixed. It is also shown that NOMA always achieves equal or higher max-min throughput than OMA-II. The performance gain of NOMA over OMA becomes more pronounced as E_s increases.

Finally, Fig. 7 provides the max-min throughput perfor-

mances versus the UAV height of different schemes for $E_U = 20$ KJ and $E_s = 10$ J. It is observed that the performance of all considered schemes decreases with the increase of H . This is expected since we assume the deterministic LoS channel model, the A2G channel conditions become weaker when the UAV flies at a higher altitude. It is also observed that the performance degradation of OMA becomes more pronounced than NOMA as H increases, which also confirms the advantages of NOMA transmission scheme.

VI. CONCLUSIONS

In this paper, energy-constrained UAV data collection systems have been investigated with the employment of both OMA and NOMA transmission. The optimization problems for maximizing the minimum UAV data collection throughput from all GNs were formulated for the two MA schemes. To solve the resulting non-convex problems, two efficient AO-based algorithms were proposed. For OMA, the original problem was decomposed into two subproblems, which were alternatively solved by applying SCA technique. For NOMA, a penalty-based algorithm was developed to solve the decoding order design subproblem, while other subproblems were solved using SCA technique. Numerical results verified the effectiveness of the proposed designs compared with other benchmark schemes, and demonstrated that the max-min throughput obtained by NOMA is always larger than or equal to OMA.

There are other promising future research directions, some of which are discussed as follows. First, given the considered energy-constrained UAV data collection system, various other performance metrics can be optimized, such as the energy efficiency at both the UAV and GNs. Second, note that only one UAV was assumed in this paper, it is interesting to consider multiple UAVs, especially for the number of GNs is large. In this case, the constraints of collision avoidance among UAVs [13] and the management of multi-UAV interference should be considered, which imposes new challenging problems. Moreover, the joint design with other A2G channel models, such as angle-dependent LoS probability model [9] and Rician fading model, is another interesting but challenging topic in the future work, which may require other sophisticated machine learning tools [37] to be employed.

APPENDIX A: PROOF OF THEOREM 1

First, the partial Lagrange function of Problem (45) can be expressed as

$$\mathcal{L}(\eta^N, \mathbf{A}, \mathbf{I}, \lambda) = \eta^N + \lambda \left(\sum_{k=1}^K \sum_{m \neq k}^K (\alpha_{k,m}[n]^2 - \alpha_{k,m}[n]) \right), \quad (50)$$

where $\mathbf{A} = \{\alpha_{k,m}[n], \forall k \neq m \in \mathcal{K}, n \in \mathcal{N}\}$, $\mathbf{I} = \{I_k[n], \forall k \in \mathcal{K}, n \in \mathcal{N}\}$ and λ is the non-negative Lagrange multiplier associated with the constraint (43). Therefore, the dual problem of Problem (45) is

$$\min_{\lambda \geq 0} \max_{(\eta^N, \mathbf{A}, \mathbf{I}) \in \mathcal{D}} \mathcal{L}(\eta^N, \mathbf{A}, \mathbf{I}, \lambda) = \min_{\lambda \geq 0} \psi(\lambda), \quad (51)$$

where \mathcal{D} is the feasible set spanned by constraints (12h), (35e), (42b) and (44) and $\psi(\lambda) = \max_{(\eta^N, \mathbf{A}, \mathbf{I}) \in \mathcal{D}} \mathcal{L}(\eta^N, \mathbf{A}, \mathbf{I}, \lambda)$.

Moreover, the primal optimization problem (45) can be equivalently expressed as

$$p^* = \max_{(\eta^N, \mathbf{A}, \mathbf{I}) \in \mathcal{D}} \min_{\lambda \geq 0} \mathcal{L}(\eta^N, \mathbf{A}, \mathbf{I}, \lambda). \quad (52)$$

Due to the weak duality [36], we have the following inequalities:

$$\begin{aligned} \min_{\lambda \geq 0} \psi(\lambda) &= \min_{\lambda \geq 0} \max_{(\eta^N, \mathbf{A}, \mathbf{I}) \in \mathcal{D}} \mathcal{L}(\eta^N, \mathbf{A}, \mathbf{I}, \lambda) \\ &\geq \max_{(\eta^N, \mathbf{A}, \mathbf{I}) \in \mathcal{D}} \min_{\lambda \geq 0} \mathcal{L}(\eta^N, \mathbf{A}, \mathbf{I}, \lambda) = p^*. \end{aligned} \quad (53)$$

It is noted that $\sum_{k=1}^K \sum_{m \neq k}^K (\alpha_{k,m}[n]^2 - \alpha_{k,m}[n]) \leq 0$ for any $\mathbf{A} \in \mathcal{D}$. Thus, $\mathcal{L}(\eta^N, \mathbf{A}, \mathbf{I}, \lambda)$ is a decreasing function with respect to λ for $(\eta^N, \mathbf{A}, \mathbf{I}) \in \mathcal{D}$, which means $\psi(\lambda)$ is bounded from below by the optimal value of Problem (45). Assume that the optimal solutions to the dual problem (51) are λ^* and $(\eta^{N*}, \mathbf{A}^*, \mathbf{I}^*)$. In the following, we discuss the optimal value of the dual problem (51) and the equivalent primal problem (52) in two cases.

First, suppose that $\sum_{k=1}^K \sum_{m \neq k}^K (\alpha_{k,m}^*[n]^2 - \alpha_{k,m}^*[n]) = 0$. Since $(\eta^{N*}, \mathbf{A}^*, \mathbf{I}^*)$ are also feasible to Problem (52), we have the following inequalities:

$$p^* \geq \eta^{N*} = \mathcal{L}(\eta^{N*}, \mathbf{A}^*, \mathbf{I}^*, \lambda^*) = \psi(\lambda^*). \quad (54)$$

Based on (53) and (54), we have

$$\begin{aligned} \max_{(\eta^N, \mathbf{A}, \mathbf{I}) \in \mathcal{D}} \min_{\lambda \geq 0} \mathcal{L}(\eta^N, \mathbf{A}, \mathbf{I}, \lambda) \\ = \min_{\lambda \geq 0} \max_{(\eta^N, \mathbf{A}, \mathbf{I}) \in \mathcal{D}} \mathcal{L}(\eta^N, \mathbf{A}, \mathbf{I}, \lambda), \end{aligned} \quad (55)$$

which implies the strong duality between the equivalent primal problem (52) and the dual problem (51) holds when $\sum_{k=1}^K \sum_{m \neq k}^K (\alpha_{k,m}[n]^2 - \alpha_{k,m}[n]) = 0$. Recall from that $\mathcal{L}(\eta^N, \mathbf{A}, \mathbf{I}, \lambda)$ is a decreasing function with respect to λ , we have

$$\psi(\lambda) = p^*, \forall \lambda \geq \lambda^*. \quad (56)$$

Second, when $\sum_{k=1}^K \sum_{m \neq k}^K (\alpha_{k,m}^*[n]^2 - \alpha_{k,m}^*[n]) < 0$, $\psi(\lambda^*) = \min_{\lambda \geq 0} \psi(\lambda) \rightarrow -\infty$ due to the monotone decreasing of $\psi(\lambda)$ with respect to λ . This contradicts the inequality in (53) since p^* is a finite value.

Therefore, $\sum_{k=1}^K \sum_{m \neq k}^K (\alpha_{k,m}^*[n]^2 - \alpha_{k,m}^*[n]) = 0$ must hold at the optimal solution and the proof of Theorem 1 is completed.

REFERENCES

- [1] J. Wang, C. Jiang, Z. Han, Y. Ren, R. G. Maunder, and L. Hanzo, "Taking drones to the next level: Cooperative distributed unmanned-aerial-vehicular networks for small and mini drones," *IEEE Veh. Technol. Mag.*, vol. 12, no. 3, pp. 73–82, 2017.
- [2] Y. Zeng, R. Zhang, and T. J. Lim, "Wireless communications with unmanned aerial vehicles: opportunities and challenges," *IEEE Commun. Mag.*, vol. 54, no. 5, pp. 36–42, 2016.
- [3] M. Mozaffari, W. Saad, M. Bennis, Y. Nam, and M. Debbah, "A tutorial on UAVs for wireless networks: Applications, challenges, and open problems," *IEEE Commun. Surv. Tut.*, vol. 21, no. 3, pp. 2334–2360, 2019.
- [4] Y. Zeng, Q. Wu, and R. Zhang, "Accessing from the sky: A tutorial on uav communications for 5G and beyond," *Proc. IEEE*, vol. 107, no. 12, pp. 2327–2375, 2019.
- [5] N. H. Motlagh, M. Bagaa, and T. Taleb, "UAV-based IoT platform: A crowd surveillance use case," *IEEE Commun. Mag.*, vol. 55, no. 2, pp. 128–134, 2017.
- [6] A. Al-Hourani, S. Kandeepan, and A. Jamalipour, "Modeling air-to-ground path loss for low altitude platforms in urban environments," in *Proc. IEEE Global Commun. Conf. (GLOBECOM)*, 2014, pp. 2898–2904.
- [7] Y. Liu, Z. Qin, M. ElKashlan, Z. Ding, A. Nallanathan, and L. Hanzo, "Nonorthogonal multiple access for 5G and beyond," *Proc. IEEE*, vol. 105, no. 12, pp. 2347–2381, 2017.
- [8] Y. Cai, Z. Qin, F. Cui, G. Y. Li, and J. A. McCann, "Modulation and multiple access for 5G networks," *IEEE Commun. Surv. Tut.*, vol. 20, no. 1, pp. 629–646, 2018.
- [9] A. Al-Hourani, S. Kandeepan, and S. Lardner, "Optimal LAP altitude for maximum coverage," *IEEE Wireless Commun. Lett.*, vol. 3, no. 6, pp. 569–572, 2014.
- [10] M. Mozaffari, W. Saad, M. Bennis, and M. Debbah, "Efficient deployment of multiple unmanned aerial vehicles for optimal wireless coverage," *IEEE Wireless Commun. Lett.*, vol. 20, no. 8, pp. 1647–1650, 2016.
- [11] J. Lyu, Y. Zeng, R. Zhang, and T. J. Lim, "Placement optimization of UAV-mounted mobile base stations," *IEEE Wireless Commun. Lett.*, vol. 21, no. 3, pp. 604–607, 2017.
- [12] M. Mozaffari, W. Saad, M. Bennis, and M. Debbah, "Unmanned aerial vehicle with underlaid device-to-device communications: Performance and tradeoffs," *IEEE Trans. Wireless Commun.*, vol. 15, no. 6, pp. 3949–3963, 2016.
- [13] Q. Wu, Y. Zeng, and R. Zhang, "Joint trajectory and communication design for multi-UAV enabled wireless networks," *IEEE Trans. Wireless Commun.*, vol. 17, no. 3, pp. 2109–2121, 2018.
- [14] Y. Cai, F. Cui, Q. Shi, M. Zhao, and G. Y. Li, "Dual-UAV-enabled secure communications: Joint trajectory design and user scheduling," *IEEE J. Sel. Areas Commun.*, vol. 36, no. 9, pp. 1972–1985, 2018.
- [15] C. You and R. Zhang, "3D trajectory optimization in rician fading for UAV-enabled data harvesting," *IEEE Trans. Wireless Commun.*, vol. 18, no. 6, pp. 3192–3207, 2019.
- [16] Y. Zeng, J. Xu, and R. Zhang, "Energy minimization for wireless communication with rotary-wing UAV," *IEEE Trans. Wireless Commun.*, vol. 18, no. 4, pp. 2329–2345, 2019.
- [17] J. Gong, T. Chang, C. Shen, and X. Chen, "Flight time minimization of UAV for data collection over wireless sensor networks," *IEEE J. Sel. Areas Commun.*, vol. 36, no. 9, pp. 1942–1954, 2018.
- [18] C. Zhan and H. Lai, "Energy minimization in Internet-of-Things system based on rotary-wing UAV," *IEEE Wireless Commun. Lett.*, vol. 8, no. 5, pp. 1341–1344, 2019.
- [19] Y. Sun, D. Xu, D. W. K. Ng, L. Dai, and R. Schober, "Optimal 3D-trajectory design and resource allocation for solar-powered UAV communication systems," *IEEE Trans. Commun.*, vol. 67, no. 6, pp. 4281–4298, 2019.
- [20] Y. Liu, Z. Qin, Y. Cai, Y. Gao, G. Y. Li, and A. Nallanathan, "UAV communications based on non-orthogonal multiple access," *IEEE Wireless Commun.*, vol. 26, no. 1, pp. 52–57, 2019.
- [21] M. F. Sohail, C. Y. Leow, and S. Won, "Non-orthogonal multiple access for unmanned aerial vehicle assisted communication," *IEEE Access*, vol. 6, pp. 22 716–22 727, 2018.
- [22] T. Hou, Y. Liu, Z. Song, X. Sun, and Y. Chen, "Multiple antenna aided NOMA in UAV networks: A stochastic geometry approach," *IEEE Trans. Commun.*, vol. 67, no. 2, pp. 1031–1044, 2019.
- [23] W. Mei and R. Zhang, "Uplink cooperative NOMA for cellular-connected UAV," *IEEE J. Sel. Topics Signal Process.*, vol. 13, no. 3, pp. 644–656, 2019.
- [24] R. Duan, J. Wang, C. Jiang, H. Yao, Y. Ren, and Y. Qian, "Resource allocation for multi-UAV aided IoT NOMA uplink transmission systems," *IEEE Internet Things J.*, vol. 6, no. 4, pp. 7025–7037, 2019.
- [25] F. Cui, Y. Cai, Z. Qin, M. Zhao, and G. Y. Li, "Multiple access for mobile-UAV enabled networks: Joint trajectory design and resource allocation," *IEEE Trans. Commun.*, vol. 67, no. 7, pp. 4980–4994, 2019.
- [26] N. Zhao, X. Pang, Z. Li, Y. Chen, F. Li, Z. Ding, and M. Alouini, "Joint trajectory and precoding optimization for UAV-assisted NOMA networks," *IEEE Trans. Commun.*, vol. 67, no. 5, pp. 3723–3735, 2019.
- [27] X. Mu, Y. Liu, L. Guo, and J. Lin, "Non-orthogonal multiple access for air-to-ground communication," *IEEE Trans. Commun.*, vol. 68, no. 5, pp. 2934–2949, 2020.

- [28] N. Zhao, Y. Li, S. Zhang, Y. Chen, W. Lu, J. Wang, and X. Wang, "Security enhancement for NOMA-UAV networks," *IEEE Trans. Veh. Technol.*, vol. 69, no. 4, pp. 3994–4005, 2020.
- [29] X. Pang, J. Tang, N. Zhao, X. Zhang, and Y. Qian, "Energy-efficient design for mmWave-enabled NOMA-UAV networks," *Sci. China Inf. Sci.*, vol. 64, no. 4, p. 140303, 2021.
- [30] 3GPP-TR-36.777, "Study on enhanced LTE support for aerial vehicles," 2017, 3GPP technical report.[Online]. Available:www.3gpp.org/dynareport/36777.htm.
- [31] D. W. Matolak and R. Sun, "Air-ground channel characterization for unmanned aircraft systems-part III: The suburban and near-urban environments," *IEEE Trans. Veh. Technol.*, vol. 66, no. 8, pp. 6607–6618, 2017.
- [32] U. Mengali and A. N. D'Andrea, *Synchronization Techniques for Digital Receivers*. New York, NY, USA: Springer, 1997.
- [33] R. Ratasuk, N. Mangalvedhe, Z. Xiong, M. Robert, and D. Bhatoolaul, "Enhancements of narrowband IoT in 3GPP Rel-14 and Rel-15," in *Proc. IEEE Conf. Stand. Commun. Netw. (CSCN)*, 2017, pp. 60–65.
- [34] Z. Chen, Z. Ding, X. Dai, and R. Zhang, "An optimization perspective of the superiority of NOMA compared to conventional OMA," *IEEE Trans. Signal Process.*, vol. 65, no. 19, pp. 5191–5202, 2017.
- [35] M. Grant and S. Boyd, "CVX: Matlab software for disciplined convex programming, version 2.1," [Online]. Available:<http://cvxr.com/cvx>, Mar 2014.
- [36] S. Boyd and L. Vandenberghe, *Convex Optimization*. Cambridge, U.K.: Cambridge Univ. Press, 2004.
- [37] X. Liu, M. Chen, Y. Liu, Y. Chen, S. Cui, and L. Hanzo, "Artificial intelligence aided next-generation networks relying on UAVs," *IEEE Wireless Commun.*, vol. 28, no. 1, pp. 120–127, 2021.